



Research paper

Synthesis, structure-activity relationship and *in vitro* pharmacodynamics of A-ring modified caged xanthenes in a preclinical model of inflammatory breast cancer

Oraphin Chantarasiwong^{a, b, 1}, Andrew T. Milcarek^{c, 1}, Theodore Habarth Morales^d, Aspen L. Settle^d, Celso O. Rezende Jr.^a, Bashayer D. Althufairi^a, Maria A. Theodoraki^{d, ***}, Mary L. Alpaugh^{c, **}, Emmanuel A. Theodorakis^{a, *}

^a Department of Chemistry and Biochemistry, University of California, 9500 Gilman Drive, La Jolla, San Diego, CA, 92093-0358, USA

^b Department of Chemistry, Faculty of Science, King Mongkut's University of Technology Thonburi, 126 Pracha Uthit Rd., Bang Mod, Thung Khru, Bangkok, 10140, Thailand

^c Department of Molecular and Cellular Biosciences, Rowan University, Glassboro, NJ, 08028, USA

^d Department of Biology, Arcadia University, Glenside, PA, 19038, USA

ARTICLE INFO

Article history:

Received 12 January 2019

Received in revised form

14 February 2019

Accepted 14 February 2019

Available online 20 February 2019

Keywords:

Spheroids

Natural product

Synthetic methods

Apoptosis

Breast cancer

ABSTRACT

Inflammatory breast cancer (IBC) is a highly metastatic, lethal form of breast cancer that lacks targeted therapeutic strategies. Inspired by the promising cytotoxicity of gambogic acid and related caged xanthenes in spheroids^{MARY-X}, an *in vitro* preclinical IBC model, we constructed a library of synthetic analogs and performed structure-activity relationship studies. The studies revealed that functionalizing the A-ring of the caged xanthone framework can significantly affect potency. Specifically, introduction of hydroxyl or fluorine groups at discrete positions of the A-ring leads to enhanced cytotoxicity at sub-micromolar concentrations. These compounds induce complete dissolution of spheroids^{MARY-X} with subsequent apoptosis of both the peripherally- and centrally-located cells, proliferative and quiescent-prone (e.g. hypoxic), respectively. These results highlight the structural flexibility and pharmacological potential of the caged xanthone motif for the design of IBC-targeting therapeutics.

© 2019 Elsevier Masson SAS. All rights reserved.

1. Introduction

Tropical trees of the genus *Garcinia* (Clusiaceae), grown mostly in Southeast Asia, India, Africa and Brazil, are widely known not only for their high value as sources of food but also for their role in ethnomedicine [1–3]. For instance, gamboge, the dried resin from *Garcinia hanburyi*, has been used in traditional Eastern medicine for its anti-infective and anti-parasitic properties [4,5]. Efforts to isolate the bioactive constituents of gamboge led to the identification of gambogic acid (**GBA**, **1**) (Fig. 1), a caged xanthonoid that displays potent anticancer activities both *in vitro* and *in vivo* [6–10] and presents a promising therapeutic window for clinical

applications [11–14]. In fact, GBA has entered clinical trials in China for the treatment of non-small cell lung, colon and renal cancers [15–17].

By virtue of its unusual chemical architecture, **GBA** has become the archetype of a family of bioactive natural products that are commonly referred to as caged xanthenes (**CXs**) [18–21]. Several members of this family exhibit potent activity against leukemia, glioblastoma, lung cancer and colorectal cancer cell lines [22–24]. Central to their structure is a xanthone framework in which the C ring has been converted into a caged motif. Plant-specific oxidations and functionalizations of this framework contribute to the structural diversity of this family. The pharmacological promise of **CXs** has inspired several structure-function studies [25–30]. These efforts unveiled that cluvenone (**2**, **CLV**) represents the minimum pharmacophore of the **CX** family [31–33] and suggested that A-ring functionalization could lead to analogs with improved bioactivity [34–38]. Along these lines, **MAD28** (**3**), the C6-hydroxylated cluvenone, was found to be approximately 3 times more active than **MAD44** (**4**), the C18-hydroxylated cluvenone (Fig. 1), in inhibiting

* Corresponding author.

** Corresponding author.

*** Corresponding author.

E-mail addresses: theodorakim@arcadia.edu (M.A. Theodoraki), alpaugh@rowan.edu (M.L. Alpaugh), etheodorakis@ucsd.edu (E.A. Theodorakis).

¹ The authors contributed equally.

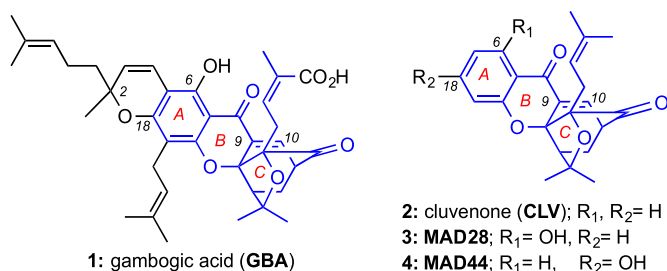


Fig. 1. Chemical structures of representative caged xanthenes: gambogic acid (GBA), cluvenone (CLV), MAD28 and MAD44.

growth in a T-cell acute lymphoblastic leukemia (CEM) cell line [39]. More recently, MAD28 (1.25 μ M) was shown to exhibit selective cytotoxicity against human epithelial breast cancer cells (MDA-MB-231 or MCF7) with no apparent detrimental effect in normal breast cells (MCF10A) [40].

The promising activity of MAD28 against breast cancer led us to evaluate its cytotoxicity in spheroids^{MARY-X}, a 3-dimensional multicellular system formed from a patient-derived xenograft of inflammatory breast cancer (IBC) [41]. IBC is a highly aggressive and often lethal subtype of breast cancer accounting for about 3–10% of diagnosed breast carcinomas [42–46]. Its high mortality rate is due to its metastatic nature and triple negative signature that renders IBC resistant to chemotherapeutic regimens [47–49]. Additionally, IBC lacks molecular markers making diagnosis and design of targeted therapeutic approaches very challenging. It is accepted that the lymphovascular embolus is a marker of cancer aggressiveness, recurrence, metastatic progression and therapeutic failure in many tumor types [50–53]. The spheroids^{MARY-X} maintain the 3-dimensional and pathophysiological features of the lymphovascular embolus [54]. As such, they provide a relevant model to test efficacy of therapeutics to IBC and metastatic disease in general. We found that both GBA and MAD28 induce spheroid dissolution and cell death in the spheroids^{MARY-X} assay with IC₅₀ values of 0.42 and 0.66 μ M, respectively [41]. Importantly, this activity was 20-fold greater than that observed with taxol (IC₅₀ = 7.8 μ M) while other FDA-approved drugs failed to induce any response [41].

In this study, we synthesized and evaluated a library of caged xanthenes in which the A-ring has been chemically modified and found that such functionalizations substantially modulate the observed cytotoxicity in the spheroids^{MARY-X} assay. Notably, attachment of electron withdrawing groups at the A-ring as well as introducing a free hydroxyl group at C6 enhances cytotoxicity and results in complete dissolution with subsequent apoptosis of the spheroids^{MARY-X} at submicromolar concentrations. Spatial/temporal analysis of the multicellular IBC spheroid showed pyknotic nuclei throughout as well as activation of PARP (i.e. cleaved PARP) at 3 h, an indication of irreversible apoptosis. Fluorescent overlay analysis of cPARP and the proliferation marker Ki67 indicated that these compounds induce apoptosis irrespective of proliferation status. Specifically, they target both the peripherally-located proliferative cells as well as the centrally-located quiescent-prone (e.g. hypoxic) cells of the multicellular spheroid. The latter represents the often resistant and chemo-refractory cell population of this disease. Thus, the caged xanthone motif represents a promising platform for future preclinical development of IBC-targeted therapeutics.

2. Results and discussion

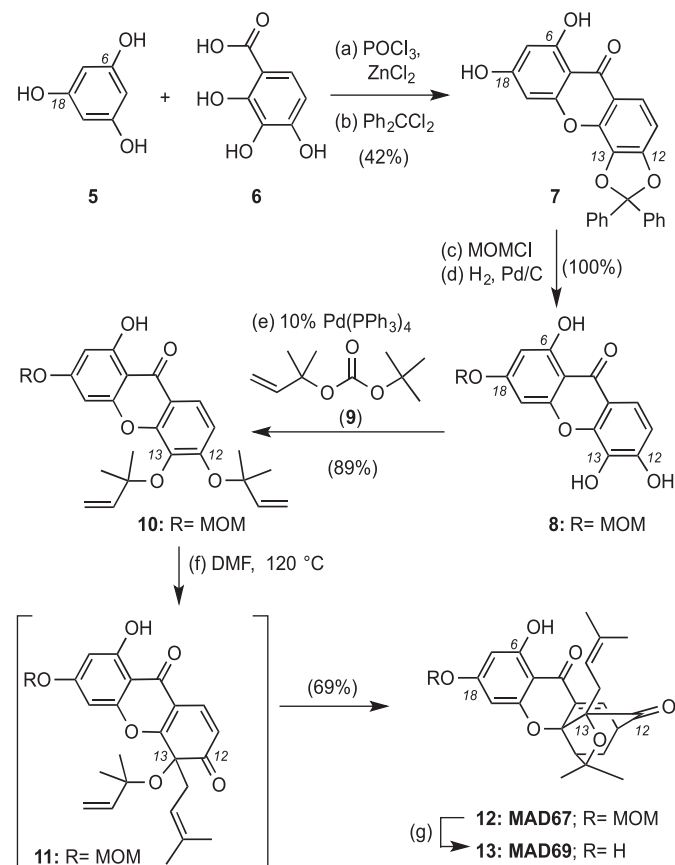
2.1. Synthesis of A-ring modified caged xanthenes

The synthesis of the C6,C18-dihydroxylated caged xanthenes **12**

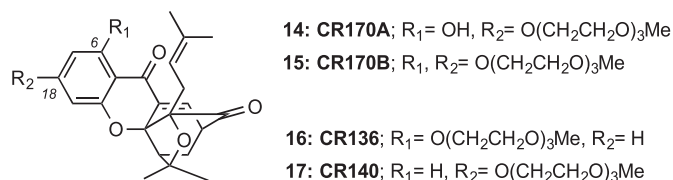
and **13** is shown in Scheme 1. Condensation of phloroglucinol (**5**) with 2,3,4-trihydroxybenzoic acid (**6**) under ZnCl₂/POCl₃ conditions [55] produced a tetrahydroxylated xanthone that was subsequently protected with diphenyldichloromethane to form compound **7** (42% yield over two steps) [56]. Selective protection of the more reactive C18-phenol with MOMCl/DIPEA followed by deprotection of the diphenyl ketal (H₂, Pd/C) gave rise to xanthone **8** (100% yield over two steps). Pd-catalyzed reverse prenylation of **8** with carbonate **9** [35] produced **10** in 89% yield. Heating of **10** in DMF at 120 °C resulted in a site-selective Claisen rearrangement of the C12-allyl ether to form intermediate **11** that underwent an intramolecular Diels-Alder cyclization to produce caged xanthone MAD67 (**12**) (69% yield over two steps) [57]. Acid-catalyzed deprotection of the C18-MOM group then gave rise to MAD69 (**13**) [37].

Treatment of **13** with tri(ethylene glycol) monomethyl ether tosylate resulted in the formation of compounds **14** and **15** in variable yields (Scheme 2) [58]. Monoalkylated compound **14** was isolated as the only product when the reaction was performed at room temperature, likely due to the higher reactivity of the C18 phenol. On the other hand, at 80 °C the reaction gave rise to dialkylated product **15** in 55% yield. Under similar conditions, caged xanthenes **3** and **4** [39] were converted to derivatives **16** and **17**, respectively.

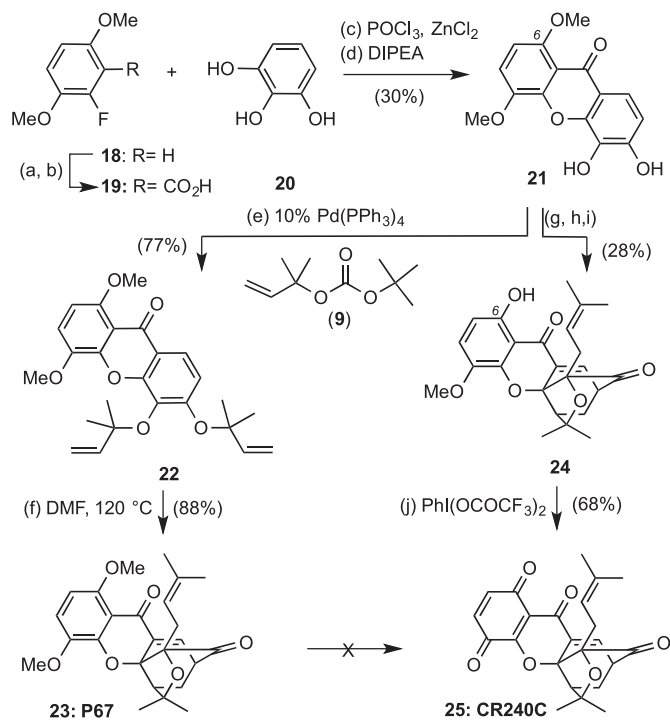
The synthesis of the caged xanthenes **23** and **25** is shown in Scheme 3. Treatment of commercially available 2-fluoro-1,4-dimethoxybenzene (**18**) with *n*-BuLi and methyl chloroformate



Scheme 1. Reagents and conditions: (a) 27 equiv. POCl₃, 10 equiv. ZnCl₂, 4.5 h, 65 °C, 62%; (b) 3 equiv. Ph₂CCl₂, acetonitrile, MW, 12 min, 150 °C, 67%; (c) 2 equiv. MOMCl, 3 equiv. DIPEA, CH₂Cl₂, 1 h, 25 °C, 100%; (d) H₂, 10% Pd/C, THF/MeOH (3:1), 18 h, 25 °C, 100%; (e) 10 equiv. *t*-butyl 2-methylbut-3-en-2-yl carbonate (**9**), 10 mol% Pd(PPh₃)₄, THF, 2 h, 0 °C, 89%; (f) DMF, 4 h, 120 °C, 69%; (g) 15% HCl, acetone, 24 h, 25 °C, 32%.



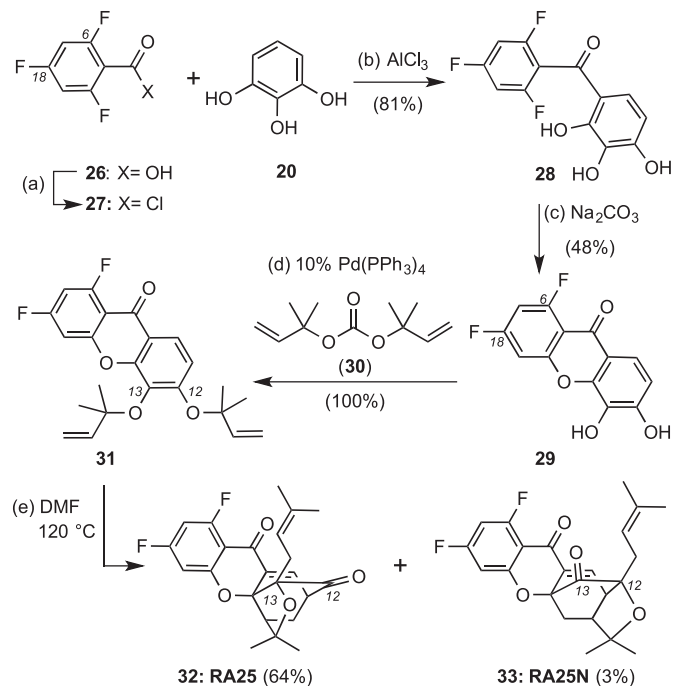
Scheme 2. Reagents and conditions: **14:** 1 equiv. **13**, 2 equiv. K₂CO₃, 2 equiv. TsO(CH₂CH₂O)₃Me, DMF, 8 h, 25 °C, 75%; **15:** 1 equiv. **13**, 3 equiv. K₂CO₃, 3 equiv. TsO(CH₂CH₂O)₃Me, DMF, 10 h, 80 °C, 55%; **16:** 1 equiv. **3**, 2 equiv. K₂CO₃, 3 equiv. TsO(CH₂CH₂O)₃Me, DMF, 8 h, 25 °C, 68%; **17:** 1 equiv. **4**, 2 equiv. K₂CO₃, 2 equiv. TsO(CH₂CH₂O)₃Me, DMF, 8 h, 80 °C, 86%.



Scheme 3. Reagents and conditions: (a) 1.2 equiv. 1.6 M *n*-BuLi, THF, 1 h, −78 °C; then 1.2 equiv. ClCO₂CH₃, THF, 4 h, −78 °C, 96%; (b) 5 equiv. LiOH, MeOH/H₂O (3:1), 1.5 h, 70 °C, 100%; (c) 1 equiv. pyrogallol (**20**), 27 equiv. POCl₃, 10 equiv. ZnCl₂, 2.5 h, 65 °C, 40%; (d) 5 equiv. DIPEA, ACN, MW, 22 min, 180 °C, 74%; (e) 10 equiv. *t*-butyl 2-methylbut-3-en-2-yl carbonate (**9**), 10 mol% Pd(PPh₃)₄, THF, 24 h, 0 °C, 77%; (f) DMF, 4 h, 120 °C, 88%; (g) 1 equiv. BBr₃ (1 M in CH₂Cl₂), CH₂Cl₂, 2 h, 0 °C–25 °C, 62%; (h) 10 equiv. *t*-butyl 2-methylbut-3-en-2-yl carbonate (**9**), 10 mol% Pd(PPh₃)₄, THF, 18 h, 0 °C, 63%; (i) DMF, 4 h, 120 °C, 72%; (j) 1.2 equiv. PhI(OAcCF₃)₂, CH₂Cl₂, 1 h, −78 °C to −30 °C, 68%.

afforded, after ester deprotection, the corresponding carboxylic acid **19** (96% combined yield) [59]. A two-step condensation of **19** with pyrogallol (**20**) produced xanthone **21** in 30% combined yield. This compound was subsequently allylated with **9** under Pd (0) catalysis and the resulting adduct **22** was rearranged to caged xanthone **23** via a Claisen/Diels-Alder reaction cascade. Various conditions, e.g. PhI(OAcCF₃)₂ or cerium ammonium nitrate, were evaluated for the *in situ* oxidative demethylation of **23** to **25** but they proved to be unsuccessful [60]. To overcome this issue, we sought to accomplish this conversion in two distinct steps [61,62]. Along these lines, we converted **21** to **25** via: (a) boron tribromide induced demethylation of the C6 methyl ether; (b) Pd (0) mediated allylation of the resulting xanthone with **9**; (c) Claisen/Diels-Alder rearrangement; and (d) PhI(OAcCF₃)₂-mediated oxidative demethylation of the resulting caged xanthone **24** (19% combined yield).

The synthesis of A-ring fluorinated caged xanthenes is described in Scheme 4. Xanthone **29** containing fluorine at C6 and C18 was



Scheme 4. Reagents and conditions: (a) 2 equiv. (COCl)₂, DMF (cat.), CH₂Cl₂, 3 h, 0 °C–25 °C, 100%; (b) 1 equiv. **20**, 3 equiv. AlCl₃, CHCl₃/CH₂Cl₂ (1:2.5), 18 h, 25 °C; then 24 h, 60 °C, 81%; (c) 1 equiv. Na₂CO₃, DMF, 3 h, 90 °C, 48%; (d) 10 equiv. bis(2-methylbut-3-en-2-yl) carbonate (**30**), 10 mol% Pd(PPh₃)₄, THF, 40 min, 5 °C, 100%; (e) DMF, 1 h, 120 °C, 64% for **32**, 3% for **33**.

prepared via: (a) conversion of 2,4,6-trifluoro benzoic acid (**26**) to its acyl chloride **27**; (b) Friedel-Crafts acylation of **27** with pyrogallol (**20**); and (c) intramolecular nucleophilic aromatic substitution of the resulting benzophenone **28** (39% combined yield, Scheme 4). Pd (0)-catalyzed reverse prenylation of **29** with carbonate **30** gave xanthone **31**. In the final step, heat-induced Claisen/Diels-Alder reaction cascade produced the regular caged xanthone **32** in 64% yield accompanied by a small amount of the neo cage isomer **33** (3% yield).

2.2. Screening of caged xanthenes using the spheroids^{MARY-X} assay

The activity of the synthetic caged xanthenes was determined using the spheroids^{MARY-X} assay. This system allows quick assessment of the drug response via brightfield microscopy and ImageJ circularity analysis (see Fig. S1, Supplemental Information), where spheroid dissolution is displayed as a deviation from the well-circumscribed spheroid edge which correlates with induction of apoptosis (i.e. drug response) [41,63]. Briefly, 30–50 spheroids^{MARY-X} were seeded in a multi-well plate and treated with increasing doses of each compound or DMSO (vehicle) for 24 h. All the compounds were tested at five different concentrations, ranging from 0.5 μM to 2.5 μM. **CX** analogs that showed no response (NR), low response (LR) and moderate response (MR) at the highest concentration (2.5 μM) are presented in Fig. 2. **MAD69** and **CR240C** showed no response (NR) as there was no deviation of the well-circumscribed edge of the spheroids^{MARY-X} comparable to the vehicle only (DMSO, control) treated spheroids^{MARY-X} (Fig. S1). Analogs **MAD44** and **P67** showed low response (LR) while **CR140**, **CR170B** showed low to moderate response (LR-MR); both pairs of drugs resulted in only minor deviations from the well-circumscribed spheroid edge. In contrast, the extent of the deviation was increased for spheroids^{MARY-X} treated with **CR170A** and **CR136** leading to a moderate response (MR).

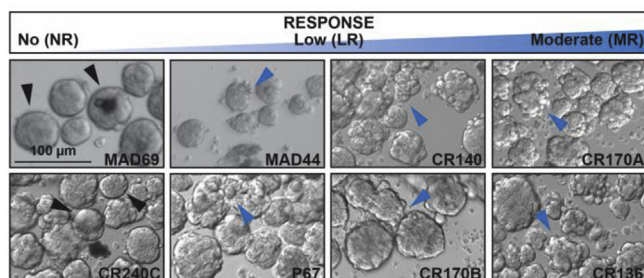


Fig. 2. Screening of A-ring modified caged xanthenes in spheroids^{MARIY-X}. Brightfield images of spheroids^{MARIY-X} after 24 h of treatment with 2.5 μM show a gradation of drug response from no deviation (black arrowheads) from well-circumscribed spheroid edge to an increase in deviation (blue arrowheads) and loss of well-circumscribed spheroid edge, as follows: **MAD69**, **CR240C**: no response (NR); **MAD44**, **P67**: low response (LR); **CR140**, **CR170B**: low response to moderate response (LR-MR); and **CR170A**, **CR136**: moderate response (MR). (For interpretation of the references to color in this figure legend, the reader is referred to the Web version of this article.)

Out of the thirteen caged xanthenes tested, five exhibited complete response (CR) as evidenced by a total dissolution of the spheroids^{MARIY-X} after 24 h treatment at 2.5 μM . Specifically, **MAD28**, **MAD67**, **CLV**, **RA25** and **RA25N** induced complete response (CR) leading to a single cell suspension of the formerly intact, well-circumscribed spheroids^{MARIY-X}. These analogs were subjected to a separate, more detailed screening, aiming to quantify their effect on spheroids^{MARIY-X} and determine their IC_{50} values. During this second screening, nine concentrations from 0.25 μM to 2.25 μM at 0.25 μM dose intervals of each compound were generated by serial dilutions and were used to treat the spheroids^{MARIY-X} for 24 h. The effect of these compounds in four representative concentrations (0.5, 0.75, 1.0 and 2.0 μM) is shown in Fig. 3 (the entire 9-concentration panel is shown in Supplemental Information; Fig. S2). The brightfield images acquired from this screening were further analyzed using ImageJ software [64] in order to quantify the circularity/response of the spheroids^{MARIY-X} and construct a dose-response graph that allows for calculation of IC_{50} values (Fig. 4).

2.3. Structure-activity relationship study

Comparison of **CLV** ($\text{IC}_{50} = 0.63 \mu\text{M}$) and **MAD28** ($\text{IC}_{50} = 0.51 \mu\text{M}$) indicates enhancement of cytotoxicity when there is a free OH group at the C6 center of the A-ring of the **CX** scaffold (Table 1). Alkylation of this group decreases the cytotoxicity as shown with **CR136** (MR) and also with **P67** (LR). These results may be due to an intramolecular hydrogen bonding between the C6-OH and the near carbonyl group that, in turn, increases the electrophilicity of the C10 enone. On the other hand, installation of a free OH group at C18 substantially reduces the cytotoxicity as shown in both **MAD44** and **MAD69** (LR and NR, respectively). In the latter structure, even the presence of an OH group at C6 is not sufficient to induce cytotoxicity. Alkylating the free C18 phenol group partially enhances the cytotoxicity as shown by comparing **CR170B** (LR-MR) to **MAD69** (NR) as well as **MAD44** (LR) to **CR140** (LR-MR). Moreover, when the C18 phenol is alkylated, the presence of a free OH group at the C6 center improves activity as shown by comparing **CR170A** (MR) to **CR170B** (LR-MR). In fact, **MAD67** that contains a MOM-protected C18 phenol and a free C6 hydroxyl group induces complete response (CR; i.e. leads to a single cell suspension of the formerly intact, well-circumscribed spheroids^{MARIY-X}) and has the highest cytotoxicity ($\text{IC}_{50} = 0.38 \mu\text{M}$).

Conversion of the A-ring phenol to a quinone leads to complete loss of activity as shown with **CR240C** (NR) indicating that the A-ring should maintain its aromatic character. On the other hand,

replacement of hydrogens with fluorines at the A-ring maintains the CR phenotype but leads to a slight decrease of the cytotoxicity as shown by comparing the difluorinated analogs **RA25** ($\text{IC}_{50} = 1.12 \mu\text{M}$) and **RA25N** ($\text{IC}_{50} = 0.89 \mu\text{M}$) to **CLV** ($\text{IC}_{50} = 0.63 \mu\text{M}$). The finding that both **RA25** and **RA25N** induce complete response (CR) and have similar cytotoxicity ($\text{IC}_{50} = 1.12 \mu\text{M}$ and 0.89 μM , respectively) indicates that both isomeric forms of the caged motif have comparable activity. Similar observations have been reported when comparing other caged xanthenes that contain regular versus neo caged structures [65,66].

2.4. Evaluation of the spatial and temporal induction of apoptosis in spheroids^{MARIY-X} by selected caged xanthenes

The spheroids^{MARIY-X} is a spontaneously-forming 3-dimensional model system that accurately recapitulates the growth, behavior and microenvironment of solid tumors [67–72]. To investigate whether the lead compounds can target any cell of the multicellular spheroid or are restricted to targeting a specific cell subpopulation, we evaluated the status of proliferation and apoptosis within the spheroids using immunofluorescence. For this experiment, the spheroids^{MARIY-X} were suspended in an extracellular matrix (ECM) plug, which provides a scaffold that prevents dispersion of the cells during drug treatment. The ECM plugs containing spheroids^{MARIY-X} were then exposed to 2.5 μM of **MAD28**, **MAD67** and **RA25**, or DMSO (control) and monitored using brightfield microscopy for loss of the well-circumscribed spheroid edge. Treatment was terminated after 3 h, when deviations from the well-circumscribed spheroid edge of all compound-treated spheroids were detected (Fig. 5; brightfield column, white arrowheads). The ECM plugs of vehicle only (DMSO) and compound-treated samples were then fixed and stained with the nuclear stain, 4',6-diamidino-2'-phenylindole dihydrochloride (DAPI), and immunostained with the apoptotic marker, cleaved fragment of poly (ADP-ribose) polymerase (cPARP) and the proliferative marker Ki67 (Fig. 5). Spheroids treated with vehicle only (DMSO) were found to have intact nuclei (i.e. viable cells) as shown with DAPI staining in sections corresponding to the middle of the spheroids. However, treatment for 3 h with 2.5 μM of **MAD28**, **MAD67**, and **RA25** was sufficient to induce apoptosis, as shown by the appearance of pyknotic nuclei (Fig. 5; DAPI column, white arrowheads). These pyknotic nuclei correlate to the loss of well-circumscribed edges in all three compound-treated samples (Fig. 5; brightfield column, white arrowhead). Pyknotic nuclei were detected both in cells on the periphery and the center of the spheroid. This indicates that not only can the compounds effectively target the peripherally-located proliferative cells but also the centrally-located, quiescent-prone cells of the spheroids. Detection of cPARP after treatment with all three compounds, suggests that 3 h of treatment at 2.5 μM is adequate to activate caspases and irreversible initiation of apoptosis throughout the spheroid (Fig. 5; cPARP column). Staining with Ki-67, a commonly used proliferation marker, and fluorescent overlay analysis (i.e. induction of apoptosis vs. proliferation status) shows that **MAD28**, **MAD67** and **RA25** target all cells of the multicellular spheroid and thus are efficacious irrespective of proliferation status (Fig. 5; Ki67 column). This impartial cancer cell targeting is clearly advantageous over the effect of various FDA-approved anticancer drugs that mainly target proliferating cells [40,41,73,74].

3. Conclusions

We report here the synthesis of a library of caged xanthenes and their *in vitro* evaluation in spheroids^{MARIY-X}, a preclinical model of inflammatory breast cancer. The synthetic strategy starts with acid-

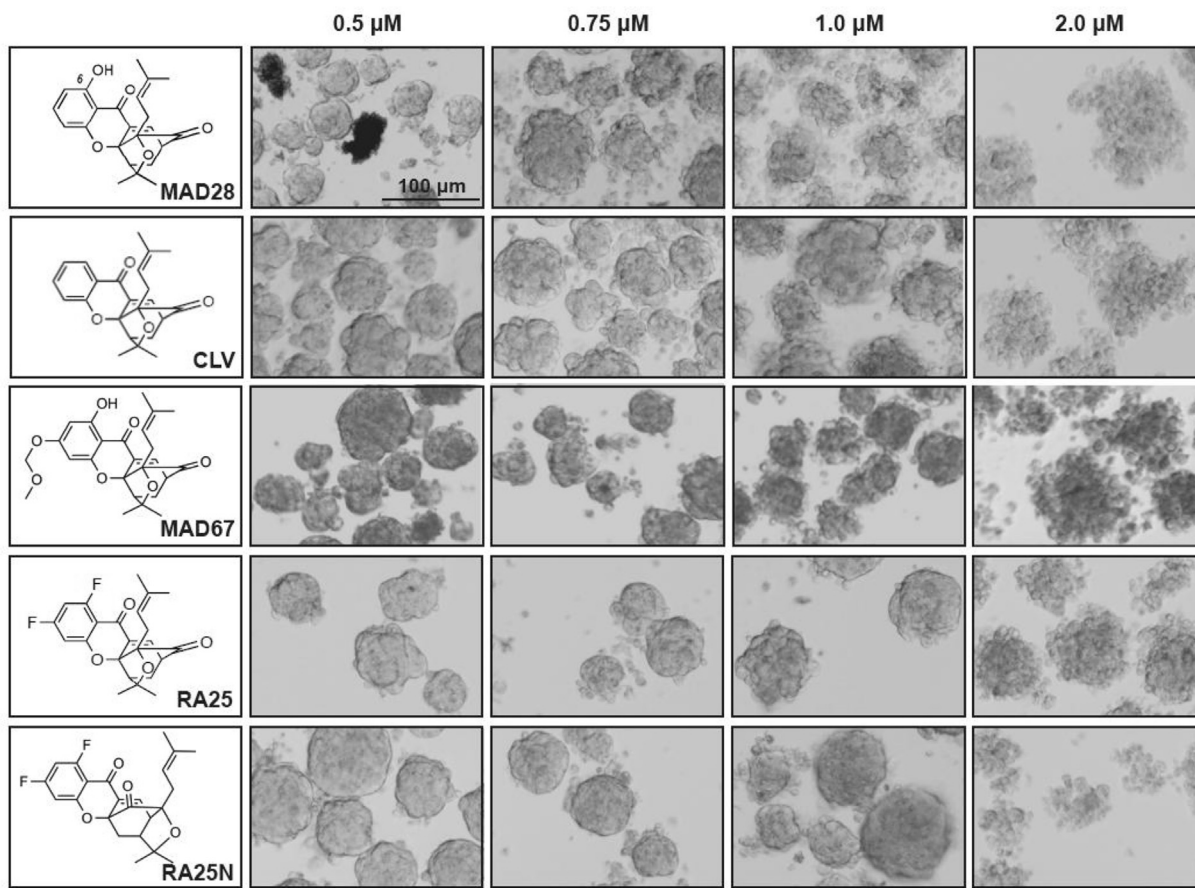


Fig. 3. Dose-dependent response of spheroids^{MARY-X} upon treatment with **MAD28**, **CLV**, **MAD67**, **RA25** and **RA25N**. Representative brightfield images of spheroids^{MARY-X} 24 h post drug treatment at 0.5, 0.75, 1.0 and 2.0 μM concentrations (bar 100 μm).

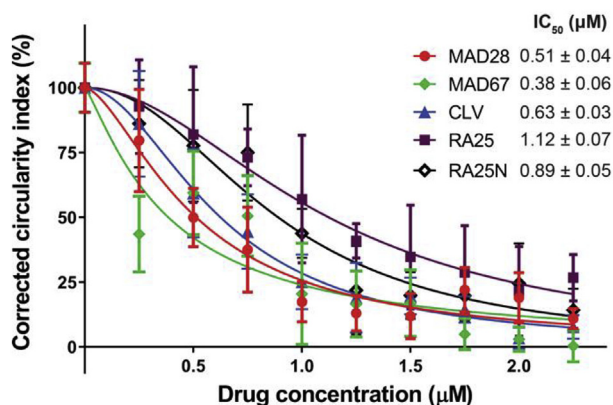


Fig. 4. Dose-response curves and IC_{50} values of CX analogs inducing complete response. Circularity values obtained via ImageJ analysis were used to calculate the IC_{50} values for **MAD28**, **MAD67**, **CLV**, **RA25** and **RA25N**. The non-linear fit curves and calculation of IC_{50} value for each analog were performed using GraphPad Prism.

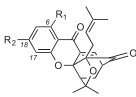
induced condensation of two appropriately functionalized aromatic rings to form the central xanthone motif that is then converted to the caged structure using the Claisen Diels-Alder reaction cascade. The overall strategy proceeds in 5–6 steps and delivers A-ring modified analogs in good yields. Structure-activity relationship studies reveal that the cytotoxicity in the spheroids^{MARY-X} assay can be regulated by selective functionalization of the A-ring. Notably, introduction of a free hydroxyl group at the C6 position leads to

compounds that exhibit complete response in the spheroid assay at low micromolar concentrations. Specifically, **MAD28** and **MAD67** were found to induce complete dissolution of the spheroids with IC_{50} values of 0.51 and 0.38 μM , respectively. Conversely, introduction of a free hydroxyl group at C18 as well as further oxidation of the A-ring leads to a decrease in cytotoxicity as evidenced with **MAD44**, **MAD69**, **CR240C** and related structures. Exchange of hydrogen atoms with fluorines at the A-ring leads to compounds **RA25** and **RA25N** that maintain the complete response phenotype albeit at a slight increase of the effective concentration (IC_{50} values 1.12 and 0.89 μM , respectively). Additional studies in ECM-immobilized spheroids showed that **MAD28**, **MAD67** and **RA25** effectively target both proliferative (peripherally located) and quiescent-prone (centrally located) cells of the multicellular spheroid. Therefore, these compounds hold promise for the treatment of resistant and chemo-refractory quiescent cancer cells [75]. Overall, these findings can be used to accelerate and streamline the development of IBC-based therapeutics based on the caged xanthone pharmacophore.

4. Experimental section

General information for chemical purification and compounds characterization. Reactions were monitored by thin-layer chromatography (TLC) carried out on 0.25 mm E. Merck silica gel plates (60F-254) and visualized under UV light and/or by treatment with a solution of CAM or KMnO_4 stain followed by heating. Preparative thin-layer chromatography separations were carried out on 0.25 or 0.50 mm E. Merck silica gel plates (60F-254). Flash

Table 1
SAR data of CX analogs.

CX analogs	R ₁	R ₂	Response	IC ₅₀ (μM)
				
CLV	H	H	CR	0.63
MAD28	OH	H	CR	0.51
MAD44	H	OH	LR	
MAD67	OH	OMOM	CR	0.38
MAD69	OH	OH	NR	
CR170A	OH	O(CH ₂ CH ₂ O) ₃ Me	MR	
CR170B	O(CH ₂ CH ₂ O) ₃ Me	O(CH ₂ CH ₂ O) ₃ Me	LR-MR	
CR136	O(CH ₂ CH ₂ O) ₃ Me	H	MR	
CR140	H	O(CH ₂ CH ₂ O) ₃ Me	LR-MR	
P67	OMe	OMe ^a	LR	
CR240C	C=O	C=O ^a	NR	
RA25	F	F	CR	1.12
RA25N^b	F	F	CR	0.89

^a R₂ is located at the C17 center.

^b RA25 N contains a neo caged motif.

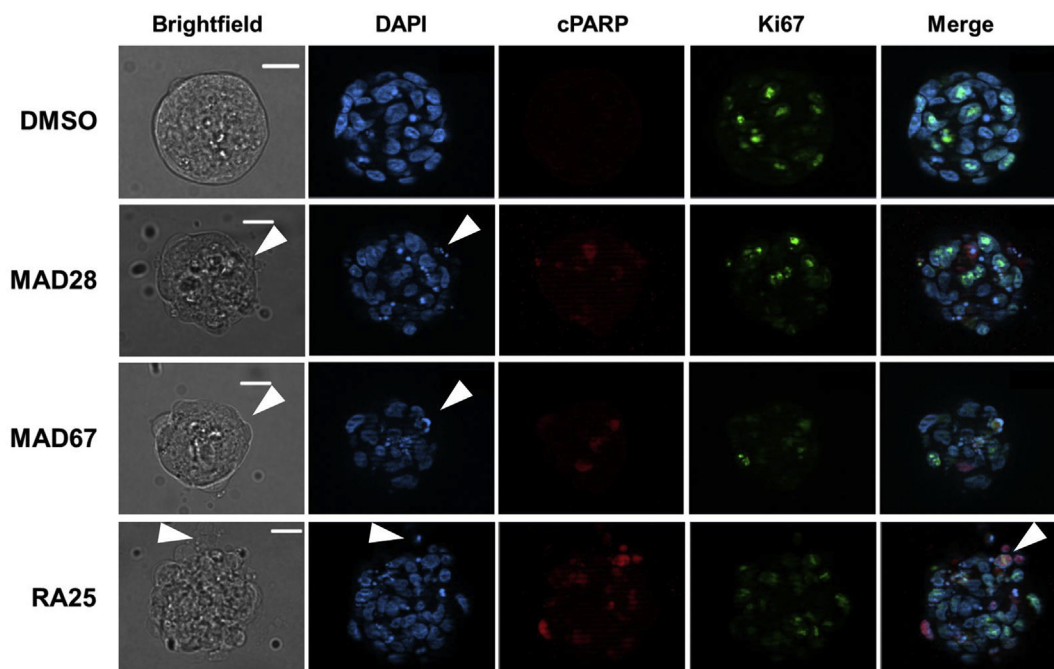


Fig. 5. Analysis of induction of apoptosis in spheroids^{MARY-X} after 3 h of treatment with **MAD28**, **MAD67** and **RA25** at 2.5 μM. Brightfield microscopy panels show the loss of well-circumscribed spheroid edge upon treatment in comparison to the control (DMSO). The immunofluorescence microscopy panels show optical slices from the middle of the spheroids^{MARY-X} and present DAPI stained nuclei (pyknotic nuclei indicated by arrowheads), localization of c-PARP, Ki-67 and the merged pictures. (bar 20 μm).

column chromatography was performed on silica gel (Merck Kieselgel 60, 230–400 mesh) using hexane/ethyl acetate or hexane/ethyl ether as standard eluents. ¹H NMR and ¹³C NMR spectra were recorded on a 400 or 500 MHz Varian or a 500 JEOL instrument. Chemical shifts (δ) are quoted in parts per million (ppm) referenced to the appropriate residual undeuterated solvent peak, with the abbreviations s, bs, d, t, q, dd, m, denoting singlet, broad singlet, doublet, triplet, quartet, doublet of doublets, multiplet, respectively. J is a coupling constant given in Hertz (Hz). High resolution mass spectra (HRMS) were recorded on a VG7070HS mass spectrometer under chemical ionization (CI) conditions, on a VG ZAB-ZSE mass spectrometer under fast atom bombardment (FAB) conditions, or on a Bruker microTOF mass spectrometer under electrospray ionization (ESI) conditions. Specific information on the

synthetic/analytical protocols as well as copies of the spectroscopic data for all compounds are shown in the Supporting Information.

General procedure for Pd(0)-catalyzed reverse prenylation. A solution of starting xanthone (1 equiv) in anhydrous THF (approximate 0.2 mM) was degassed by argon and was placed in an ice bath. To this homogeneous solution was added *tert*-butyl 2-methylbut-3-en-2-yl carbonate (**9**) or bis(2-methylbut-3-en-2-yl) carbonate (**30**) (10 equiv) via syringe, followed by 10% mol Pd(PPh₃)₄. The mixture was stirred under argon at 0–5 °C and the reaction progress was monitored by TLC. Upon completion the reaction mixture was quenched with water and extracted with EtOAc. The combined organic layers were dried over MgSO₄, filtered and concentrated by rotary evaporation. The crude material was purified through flash column chromatography (silica, EtOAc in hexane)

to yield di-allylated product.

1-hydroxy-3-(methoxymethoxy)-5,6-bis((2-methylbut-3-en-2-yl)oxy)-9H-xanthen-9-one (10): 89%, a colorless oil. $R_f = 0.57$ (25% EtOAc–hexane); $^1\text{H NMR}$ (400 MHz, CDCl_3) δ 7.82 (d, $J = 9.0$ Hz, 1H), 7.11 (d, $J = 9.0$ Hz, 1H), 6.56 (d, $J = 2.2$ Hz, 1H), 6.46 (d, $J = 2.2$ Hz, 1H), 6.29–6.14 (m, 2H), 5.25 (s, 2H), 5.21–5.15 (m, 3H), 5.03 (d, $J = 10.9$ Hz, 1H), 3.51 (s, 3H), 1.57 (s, 9H), 1.57 (s, 3H); $^{13}\text{C NMR}$ (100 MHz, CDCl_3) δ 180.9, 164.0, 163.5, 157.5, 152.5, 143.7, 143.5, 120.4, 116.8, 114.4, 113.4, 98.8, 94.9, 94.4, 83.9, 82.5, 56.7, 27.4, 27.1; HRMS calc. for $\text{C}_{25}\text{H}_{29}\text{O}_7$ (M + H) $^+$ 441.1988, found 441.1907.

1,4-dimethoxy-5,6-bis((2-methylbut-3-en-2-yl)oxy)-9H-xanthen-9-one (22): 77%, a colorless oil. $R_f = 0.43$ (50% EtOAc–hexane); $^1\text{H NMR}$ (400 MHz, CDCl_3) δ 7.87 (d, $J = 9.1$ Hz, 1H), 7.15 (d, $J = 8.9$ Hz, 1H), 7.08 (d, $J = 9.0$ Hz, 1H), 6.69 (d, $J = 9.0$ Hz, 1H), 6.41 (dd, $J = 10.7$, 17.6 Hz, 1H), 6.19 (dd, $J = 10.8$, 17.6 Hz, 1H), 5.21–5.13 (m, 3H), 4.97 (d, $J = 10.9$ Hz, 1H), 3.96 (s, 3H), 3.95 (s, 3H), 1.61 (s, 6H), 1.55 (s, 6H); $^{13}\text{C NMR}$ (100 MHz, CDCl_3) δ 176.4, 156.2, 153.6, 151.2, 148.0, 143.8, 143.7, 142.6, 135.8, 120.8, 117.2, 116.2, 113.9, 113.0, 104.2, 83.9, 82.0, 56.7, 56.5, 27.1, 26.7; HRMS calc. for $\text{C}_{25}\text{H}_{28}\text{O}_6\text{Na}$ (M + Na) $^+$, 447.1778 found 447.1777.

1,3-difluoro-5,6-bis((2-methylbut-3-en-2-yl)oxy)-9H-xanthen-9-one (31): 100%, a colorless oil. $R_f = 0.56$ (33% Et₂O–hexane); $^1\text{H NMR}$ (400 MHz, CDCl_3) δ 7.87 (d, $J = 9.1$ Hz, 1H), 7.13 (d, $J = 9.0$ Hz, 1H), 6.97 (d, $J_{\text{H,F}} = 9.1$ Hz, 1H), 6.78 (t, $J_{\text{H,F}} = 10.9$ Hz, 1H), 6.27–6.13 (m, 2H), 5.23–5.16 (m, 3H), 5.04 (d, $J = 10.8$ Hz, 1H), 1.57 (s, 6H), 1.56 (s, 6H); $^{13}\text{C NMR}$ (100 MHz, CDCl_3) δ 174.3, 166.8 (d, $J_{\text{C,F}} = 15.4$ Hz), 164.3 (dd, $J_{\text{C,F}} = 15.0$, 8.1 Hz), 161.7 (d, $J_{\text{C,F}} = 15.6$ Hz), 158.0 (d, $J_{\text{C,F}} = 15.9$ Hz), 157.4, 151.8, 143.7, 143.5, 135.4, 121.3, 117.2, 114.5, 113.4, 101.1 (d, $J_{\text{C,F}} = 25.1$ Hz), 101.0 (t, $J_{\text{C,F}} = 24.2$ Hz), 84.0, 82.6, 27.4, 27.2; HRMS calc. for $\text{C}_{23}\text{H}_{22}\text{F}_2\text{O}_4\text{Na}$ (M + Na) $^+$ 423.1378, found 423.1377.

General procedure for Claisen/Diels-Alder reaction. A solution of allylated compound (1 equiv) in DMF was heated at 120 °C. The onset of a yellow color indicated the formation of the caged xanthone. The reaction progress was monitored by TLC. Upon completion, the yellow reaction mixture was cooled to room temperature and the solvent was removed under vacuum by rotary evaporation. The crude material was purified by flash column chromatography (silica, EtOAc or Et₂O in hexane) to yield the caged xanthone.

8-hydroxy-10-(methoxymethoxy)-2,2-dimethyl-3a-(3-methylbut-2-en-1-yl)-1,2-dihydro-1,5-methanofuro[2,3-d]xanthene-4,7(3aH,5H)-dione (12): 69%, yellow solid. $R_f = 0.24$ (25% EtOAc–hexane); $^1\text{H NMR}$ (400 MHz, CDCl_3) δ 12.38 (s, 1H), 7.43 (d, $J = 7.1$ Hz, 1H), 6.20 (d, $J = 2.1$ Hz, 1H), 6.17 (d, $J = 2.1$ Hz, 1H), 5.19 (s, 2H), 4.45–4.41 (m, 1H), 3.51–3.48 (m, 1H), 3.47 (s, 3H), 2.61 (d, $J = 8.8$ Hz, 2H), 2.43 (d, $J = 9.6$ Hz, 1H), 2.33 (dd, $J = 13.6$, 4.7 Hz, 1H), 1.68 (s, 3H), 1.38 (s, 3H), 1.32–1.31 (m, 1H), 1.29 (s, 3H), 1.09 (s, 3H); $^{13}\text{C NMR}$ (100 MHz, CDCl_3) δ 203.2, 179.7, 166.1, 164.9, 161.1, 135.4, 134.2, 133.9, 118.5, 101.8, 97.2, 95.7, 94.1, 90.4, 84.6, 83.7, 56.7, 49.0, 47.0, 30.6, 29.9, 29.3, 25.8, 25.3, 17.0; HRMS calc. for $\text{C}_{25}\text{H}_{28}\text{O}_7\text{Na}$ (M + Na) $^+$ 463.1727, found 463.1729.

8,11-dimethoxy-2,2-dimethyl-3a-(3-methylbut-2-en-1-yl)-1,2-dihydro-1,5-methanofuro[2,3-d]xanthene-4,7(3aH,5H)-dione (23): 88%, yellow solid. $R_f = 0.40$ (50% EtOAc–hexane); $^1\text{H NMR}$ (400 MHz, CDCl_3) δ 7.31 (d, $J = 6.9$ Hz, 1H), 7.04 (d, $J = 9.0$ Hz, 1H), 6.47 (d, $J = 9.0$ Hz, 1H), 4.52 (t, $J = 7.9$ Hz, 1H), 3.88 (s, 3H), 3.85 (s, 3H), 3.44 (dd, $J = 7.0$, 4.2 Hz, 1H), 2.61 (d, $J = 9.0$ Hz, 2H), 2.40 (d, $J = 9.6$ Hz, 1H), 2.32 (dd, $J = 13.5$, 4.6 Hz, 1H), 1.78 (s, 3H), 1.39 (s, 3H), 1.30 (s, 3H), 1.30–1.27 (m, 1H), 1.09 (s, 3H); $^{13}\text{C NMR}$ (100 MHz, CDCl_3) δ 203.3, 176.1, 154.3, 151.2, 143.0, 136.4, 132.5, 118.7, 118.5, 110.9, 102.8, 90.0, 84.5, 83.6, 57.0, 56.4, 48.5, 46.7, 29.5, 29.1, 29.0, 25.6, 25.4, 16.9; HRMS calc. for $\text{C}_{25}\text{H}_{28}\text{O}_6\text{Na}$ (M + Na) $^+$, 447.1778 found 447.1776.

8-hydroxy-11-methoxy-2,2-dimethyl-3a-(3-methylbut-2-en-

1-yl)-1,2-dihydro-1,5-methanofuro[2,3-d]xanthene-4,7(3aH,5H)-dione (24): 72%, yellow solid. $R_f = 0.50$ (50% EtOAc–hexane); $^1\text{H NMR}$ (400 MHz, CDCl_3) δ 11.55 (s, 1H), 7.49 (d, $J = 7.0$ Hz, 1H), 7.12 (dd, $J = 8.9$, 1.8 Hz, 1H), 6.47 (dd, $J = 8.9$, 1.8 Hz, 1H), 4.43–4.39 (m, 1H), 3.84 (s, 3H), 3.55–3.52 (m, 1H), 2.64 (d, $J = 9.5$ Hz, 2H), 2.47 (d, $J = 9.6$ Hz, 1H), 2.36 (dd, $J = 13.6$, 4.2 Hz, 1H), 1.78 (s, 3H), 1.36 (s, 3H), 1.31 (s, 4H), 1.00 (s, 3H); $^{13}\text{C NMR}$ (100 MHz, CDCl_3) δ 202.8, 181.6, 156.2, 149.5, 140.7, 135.4, 135.0, 134.0, 124.1, 119.0, 107.6, 106.5, 90.4, 84.7, 84.0, 57.9, 49.0, 47.1, 29.8, 29.4, 29.3, 25.7, 24.9, 16.8; HRMS calc. for $[\text{C}_{24}\text{H}_{26}\text{O}_6\text{Na}]^+$ (M + Na) $^+$ 433.1622, found 433.1623.

8,10-difluoro-2,2-dimethyl-3a-(3-methylbut-2-en-1-yl)-1,2-dihydro-1,5-methanofuro[2,3-d]xanthene-4,7(3aH,5H)-dione (32): 64% yellow solid; $R_f = 0.38$ (50% Et₂O–hexane); $^1\text{H NMR}$ (400 MHz, CDCl_3) δ 7.42 (d, $J = 6.9$ Hz, 1H), 6.60 (d, $J_{\text{H,F}} = 9.5$ Hz, 1H), 6.53 (t, $J_{\text{H,F}} = 10.9$ Hz, 1H), 4.46 (t, $J = 6.9$ Hz, 1H), 3.52–3.49 (m, 1H), 2.60 (d, $J = 8.3$ Hz, 2H), 2.44 (d, $J = 10.0$ Hz, 1H), 2.34 (dd, $J = 13.6$, 4.6 Hz, 1H), 1.67 (s, 3H), 1.40 (s, 3H), 1.35–1.31 (m, 1H), 1.30 (s, 3H), 1.09 (s, 3H); $^{13}\text{C NMR}$ (100 MHz, CDCl_3) δ 202.7, 173.5, 168.2 (d, $J_{\text{C,F}} = 16.0$ Hz), 165.3 (dd, $J_{\text{C,F}} = 77.3$, 15.9 Hz), 162.2 (d, $J_{\text{C,F}} = 16.0$ Hz), 161.8 (dd, $J_{\text{C,F}} = 15.6$, 5.5 Hz), 135.2, 134.7, 134.5, 118.9, 101.5 (dd, $J_{\text{C,F}} = 24.6$, 4.4 Hz), 99.4 (t, $J_{\text{C,F}} = 25.5$ Hz), 91.4, 84.6, 83.7, 49.0, 47.0, 29.9, 29.3, 29.2, 25.7, 25.5, 17.2; HRMS calc. for $\text{C}_{23}\text{H}_{22}\text{F}_2\text{O}_4\text{Na}$ (M + Na) $^+$ 423.1378, found 423.1373.

6,8-difluoro-2,2-dimethyl-11a-(3-methylbut-2-en-1-yl)-2,3,3a,11a-tetrahydro-3,10a-methanofuro[3,2-b]xanthene-5,11-dione (33): 3%, yellow solid; $R_f = 0.48$ (50% Et₂O–hexane); $^1\text{H NMR}$ (400 MHz, CDCl_3) δ 7.22 (d, $J = 7.0$ Hz, 1H), 6.74 (d, $J_{\text{H,F}} = 9.6$ Hz, 1H), 6.52 (t, $J_{\text{H,F}} = 11.0$ Hz, 1H), 5.01 (t, $J = 6.9$ Hz, 1H), 3.76 (dd, $J = 6.9$, 4.7 Hz, 1H), 2.50–2.46 (m, 2H), 2.19 (dd, $J = 9.9$, 4.5 Hz, 1H), 2.12–2.04 (m, 1H), 1.87 (dd, $J = 13.2$, 10.0 Hz, 1H), 1.72 (s, 3H), 1.60 (s, 3H), 1.38 (s, 3H), 1.35 (s, 3H); $^{13}\text{C NMR}$ (100 MHz, CDCl_3) δ 199.6, 172.8, 168.5 (d, $J_{\text{C,F}} = 15.8$ Hz), 165.9 (d, $J_{\text{C,F}} = 16.1$ Hz), 162.7 (m), 162.2 (m), 136.7, 135.6, 131.8, 117.4, 102.0 (dd, $J_{\text{C,F}} = 24.9$, 4.2 Hz), 99.7 (t, $J_{\text{C,F}} = 20.0$ Hz), 85.0, 84.1, 79.2, 44.9, 42.5, 32.9, 30.3, 29.8, 26.9, 26.1, 18.4; HRMS calc. for $\text{C}_{23}\text{H}_{22}\text{F}_2\text{O}_4\text{Na}$ (M + Na) $^+$ 423.1378, found 423.1379.

Culture of spheroids^{MARY-X}. The spheroids^{MARY-X} were cultured in Minimal Essential Medium (MEM) supplemented with 10% heat-inactivated fetal bovine serum and antibiotics (100 U/ml penicillin and 100 $\mu\text{g}/\text{ml}$ streptomycin) at 37 °C in an air –5% CO₂ atmosphere at constant humidity.

Compound screening and drug response using the spheroids^{MARY-X} assay. Spheroids^{MARY-X} ranging in size from 40 to 100 μm were seeded at a density of 30–50 spheroids/well in a multi-well plate and treated in replicates with different drug concentrations or vehicle only (DMSO) as a control. Brightfield images were acquired 24 h post treatment and the response to the drugs was evaluated based on deviations from the circularity of intact, well-circumscribed spheroids^{MARY-X}. Circularity measurements for compounds that led to complete dissolution, turning the spheroids^{MARY-X} to single cell suspension were obtained using ImageJ. The parameters of the image analysis are set so that ‘1’ indicates a perfect circle (i.e. intact spheroid; no response) and numbers approaching ‘0’ indicate loss of circularity (i.e. dissolute spheroid; response). Response to drug treatment is ranked as no response, low response, moderate response or complete response, based on the degree of deviation from a well-circumscribed spheroid edge. The circularity measurements were then transferred into GraphPad Prism v. 7.04 in order to construct a dose-response curve and calculate the IC₅₀ values of each drug.

Immunofluorescence in extracellular matrix plugs. Extracellular matrix (Matrigel; Corning LifeSciences, cat.# 356237) was thawed at 4 °C overnight and kept on ice at all times during use. A mixture of matrigel with spheroids^{MARY-X} in media at a 2:1 ratio was

prepared and added on top of a glass coverslip into each well of a plate. The plate with the matrigel plugs was allowed to solidify for 30 min at 37 °C, before adding media with appropriate drug concentrations in the wells. After 3 h of treatment, the drug containing media was removed and the wells were topped off with 4% paraformaldehyde (PFA). PFA fixation proceeded for 30 min at room temperature, followed by PBS washes and 15 min permeabilization of the cells with 2% Triton X-100 in PBS. After washing twice with 1× PBS, the cells were blocked with 3% normal goat serum in 1× PBS for 30 min at room temperature. The treated cells inside the Matrigel plug were then incubated at 4 °C for 24 h with Alexa Fluor 488 conjugated anti-Ki67 (BD Pharmingen, #558616) and cPARP (Promega, #G7341) at 1:10 and 1:100, respectively. Incubation with Cy5 conjugated goat anti-rabbit (Invitrogen, A10523) secondary at 4 µg/ml followed at 4 °C for 24 h. After three washes in 1× PBS, a drop of Vectashield mounting medium with DAPI (Vector Laboratories, H-1200) was applied on top of the Matrigel plugs with the treated cells and then the coverslips were flipped and sealed on slides. The slides were visualized and subjected to z-stacking using a Zeiss AxioObserver Z1 with ApoTome2 inverted microscope.

Conflicts of interest

The authors declare no competing financial interest.

Acknowledgment

We thank the California Breast Cancer Research Program (IDEA Award No: 22IB-0024). We thank the Thailand Research Fund for a New Researcher Grant (TRG5780085) to Dr. O. Chantarasriwong and Kuwait University for a Fellowship to B.D. Althufairi. This work was also supported by the Ellington Beavers Award from Arcadia University. We also thank Teresa Abendroth for editorial assistance.

Appendix A. Supplementary data

Supplementary data to this article can be found online at <https://doi.org/10.1016/j.ejmech.2019.02.047>.

References

- [1] S. Kumar, S. Sharma, S.K. Chattopadhyay, The potential health benefit of polyisoprenylated benzophenones from *Garcinia* and related genera: ethnobotanical and therapeutic importance, *Fitoterapia* 89 (2013) 86–125.
- [2] K. Maneenoon, C. Khuniad, Y. Teanuan, N. Saedan, S. Prom-in, N. Rukleng, W. Kongpool, P. Pinsook, W. Wongwiwat, Ethnomedicinal plants used by traditional healers in Phatthalung Province, Peninsular Thailand, *J. Ethnobiol. Ethnomed.* 11 (2015).
- [3] P.W. Sweeney, Phylogeny and floral diversity in the genus *Garcinia* (clusiaceae) and relatives, *Int. J. Plant Sci.* 169 (2008) 1288–1303.
- [4] W. Wang, Y.R. Li, Y.Q. Chen, H.J. Chen, P. Zhu, M.M. Xu, H. Wang, M.N. Wu, Z.J. Yang, R.M. Hoffman, Y.F. Gu, Ethanol extract of traditional Chinese medicine (TCM) gamboge inhibits colon cancer via the wnt/beta-catenin signaling pathway in an orthotopic mouse model, *Anticancer Res.* 38 (2018) 1917–1925.
- [5] M. Xu, H.S. Tan, W.W. Fu, L.Y. Pan, Y.X. Tang, S.D. Huang, Y.F. Xiu, Simultaneous determination of seven components in gamboge and its processed products using a single reference standard, *Chin. Herb. Med.* 9 (2017) 42–49.
- [6] Q.L. Guo, Q. Qi, Q.D. You, H.Y. Gu, L. Zhao, Z.Q. Wu, Toxicological studies of gambogic acid and its potential targets in experimental animals, *Basic Clin. Pharmacol. Toxicol.* 99 (2006) 178–184.
- [7] Q. Qi, Q. You, H. Gu, L. Zhao, W. Liu, N. Lu, Q. Guo, Studies on the toxicity of gambogic acid in rats, *J. Ethnopharmacol.* 117 (2008) 433–438.
- [8] L. Qiang, Y. Yang, Q.D. You, Y.J. Ma, L. Yang, F.F. Nie, H.Y. Gu, L. Zhao, N. Lu, Q. Qi, W. Liu, X.T. Wang, Q.L. Guo, Inhibition of glioblastoma growth and angiogenesis by gambogic acid: an in vitro and in vivo study, *Biochem. Pharmacol.* 75 (2008) 1083–1092.
- [9] Y. Yang, L. Yang, Q.D. You, F.F. Nie, H.Y. Gu, L. Zhao, X.T. Wang, Q.L. Guo, Differential apoptotic induction of gambogic acid, a novel anticancer natural product, on hepatoma cells and normal hepatocytes, *Cancer Lett.* 256 (2007) 259–266.
- [10] D. Zhai, C. Jin, C.W. Shiau, S. Kitada, A.C. Satterthwait, J.C. Reed, Gambogic acid is an antagonist of antiapoptotic Bcl-2 family proteins, *Mol. Canc. Therapeut.* 7 (2008) 1639–1646.
- [11] K. Banik, C. Harsha, D. Bordoloi, B.L. Sailo, G. Sethi, H.C. Leong, F. Arfuso, S. Mishra, L.Z. Wang, A.P. Kumar, A.B. Kunnumakkara, Therapeutic potential of gambogic acid, a caged xanthone, to target cancer, *Cancer Lett.* 416 (2018) 75–86.
- [12] J. Felth, K. Lesiak-Mieczkowska, P. D'Arcy, C. Haglund, J. Gullbo, R. Larsson, S. Linder, L. Bohlin, M. Fryknas, L. Rickardson, Gambogic acid is cytotoxic to cancer cells through inhibition of the ubiquitin-proteasome system, *Invest. N. Drugs* 31 (2013) 587–598.
- [13] D. Kashyap, R. Mondal, H.S. Tuli, G. Kumar, A.K. Sharma, Molecular targets of gambogic acid in cancer: recent trends and advancements, *Tumours. Biol.* 37 (2016) 12915–12925.
- [14] L. Zhao, C. Zhen, Z. Wu, R. Hu, C. Zhou, Q. Guo, General pharmacological properties, developmental toxicity, and analgesic activity of gambogic acid, a novel natural anticancer agent, *Drug Chem. Toxicol.* 33 (2010) 88–96.
- [15] Y.H.B.L. Chi, X.K. Zhan, H. Yu, G.R. Xie, Z.Z. Wang, W. Xiao, Y.G. Wang, F.X. Xiong, J.F. Hu, L. Yang, C.X. Cui, J.W. Wang, An open-labeled, randomized, multicenter phase IIa study of gambogic acid injection for advanced malignant tumors, *Chin. Med. J.* 126 (2013) 1642–1646.
- [16] L.H. Wang, Y. Li, S.N. Yang, F.Y. Wang, Y. Hou, W. Cui, K. Chen, Q. Cao, S. Wang, T.Y. Zhang, Z.Z. Wang, W. Xiao, J.Y. Yang, C.F. Wu, Gambogic acid synergistically potentiates cisplatin-induced apoptosis in non-small-cell lung cancer through suppressing NF-kappa B and MAPK/HO-1 signalling, *Br. J. Canc.* 110 (2014) 341–352.
- [17] X. Wang, R. Deng, Y. Lu, Q. Xu, M. Yan, D. Ye, W. Chen, Gambogic acid as a non-competitive inhibitor of ATP-binding cassette transporter B1 reverses the multidrug resistance of human epithelial cancers by promoting ATP-binding cassette transporter B1 protein degradation, *Basic Clin. Pharmacol. Toxicol.* 112 (2013) 25–33.
- [18] O. Chantarasriwong, A. Batova, W. Chavasiri, E.A. Theodorakis, Chemistry and biology of the caged *Garcinia* xanthenes, *Chem. Eur. J.* 16 (2010) 9944–9962.
- [19] N. Anantachoke, P. Tuchinda, C. Kuhakarn, M. Pohmakotr, V. Reutrakul, Prenylated caged xanthenes: chemistry and biology, *Pharmaceut. Biol.* 50 (2012) 78–91.
- [20] B. Jia, S. Li, X. Hu, G. Zhu, W. Chen, Recent Research on bioactive xanthenes from natural medicine: *Garcinia hanburyi*, *AAPS PharmSciTech* 16 (2015) 742–758.
- [21] O. Chantarasriwong, B.D. Althufairi, N.J. Checchia, E.A. Theodorakis, in: R. Attaur (Ed.), *Studies in Natural Products Chemistry*, vol. 58, Elsevier, 2018, pp. 93–131.
- [22] C. Boonyong, C. Pattamadilok, R. Suttisri, S. Jianmongkol, Benzophenones and xanthone derivatives from *Garcinia schomburgkiana*-induced P-glycoprotein overexpression in human colorectal Caco-2 cells via oxidative stress-mediated mechanisms, *Phytomedicine* 27 (2017) 8–14.
- [23] C. Kaewpiboon, N. Boonnak, N. Yawut, S. Kaowinn, Y.H. Chung, Caged-xanthone from *Cratogeomys formosus* ssp. *pruniflorum* inhibits malignant cancer phenotypes in multidrug-resistant human A549 lung cancer cells through down-regulation of NF-kappaB, *Bioorg. Med. Chem.* (2018). <https://doi.org/10.1016/j.bmc.2018.12.042>.
- [24] G. Tovilovic-Kovacevic, D. Krstic-Milosevic, B. Vinterhalter, M. Toljic, V. Perovic, V. Trajkovic, L. Harhaji-Trajkovic, N. Zogovic, Xanthone-rich extract from *Gentiana dinarica* transformed roots and its active component norswertianin induce autophagy and ROS-dependent differentiation of human glioblastoma cell line, *Phytomedicine* 47 (2018) 151–160.
- [25] J. Kuemmerle, S. Jiang, B. Tseng, S. Kasibhatla, J. Drewe, S.X. Cai, Synthesis of caged 2,3,3a,7a-tetrahydro-3,6-methanobenzofuran-7(6H)-ones: evaluating the minimum structure for apoptosis induction by gambogic acid, *Bioorg. Med. Chem.* 16 (2008) 4233–4241.
- [26] X. Xu, Y. Wu, M. Hu, X. Li, Q. Bao, J. Bian, Q. You, X. Zhang, Novel natural product-like caged xanthenes bearing a carbamate moiety exhibit antitumor potency and anti-angiogenesis activity in vivo, *Sci. Rep.* 6 (2016) 35771.
- [27] X. Zhang, X. Li, H. Sun, Z. Jiang, L. Tao, Y. Gao, Q. Guo, Q. You, Synthesis and evaluation of novel aza-caged *Garcinia* xanthenes, *Org. Biomol. Chem.* 10 (2012) 3288–3299.
- [28] X. Zhang, X. Li, H. Sun, X. Wang, L. Zhao, Y. Gao, X. Liu, S. Zhang, Y. Wang, Y. Yang, S. Zeng, Q. Guo, Q. You, *Garcinia* xanthenes as orally active antitumor agents, *J. Med. Chem.* 56 (2013) 276–292.
- [29] H. Ke, J.M. Morrissey, S. Qu, O. Chantarasriwong, M.W. Mather, E.A. Theodorakis, A.B. Vaidya, Caged *Garcinia* xanthenes, a novel chemical scaffold with potent antimalarial activity *antimicrob. Agents Chemother.* 61 (2017) e01220-01216.
- [30] E.J. Tisdale, C. Chowdhury, B.G. Vong, H. Li, E.A. Theodorakis, Regioselective synthesis of the bridged tricyclic core of *Garcinia* natural products via intramolecular aryl acrylate cycloadditions, *Org. Lett.* 4 (2002) 909–912.
- [31] G. Guizzunti, A. Batova, O. Chantarasriwong, M. Dakanali, E.A. Theodorakis, Subcellular localization and activity of gambogic acid, *Chembiochem* 13 (2012) 1191–1198.
- [32] G. Guizzunti, E.A. Theodorakis, A.L. Yu, C. Zurzolo, A. Batova, Cluvenone induces apoptosis via a direct target in mitochondria: a possible mechanism to circumvent chemo-resistance? *Invest. N. Drugs* 30 (2012) 1841–1848.
- [33] A. Batova, D. Altomare, O. Chantarasriwong, K.L. Ohlsen, K.E. Creek, Y.-C. Lin, A. Messersmith, A.L. Yu, J. Yu, E.A. Theodorakis, The synthetic caged *Garcinia* xanthone cluvenone induces cell stress and apoptosis and has immune modulatory activity, *Mol. Canc. Therapeut.* 9 (2010) 2869–2878.

- [34] A. Batova, T. Lam, V. Wascholowski, A.L. Yu, A. Giannis, E.A. Theodorakis, Synthesis and evaluation of caged Garcinia xanthenes, *Org. Biomol. Chem.* 5 (2007) 494–500.
- [35] O. Chantarasriwong, W.C. Cho, A. Batova, W. Chavasiri, C. Moore, A.L. Rheingold, E.A. Theodorakis, Evaluation of the pharmacophoric motif of the caged Garcinia xanthenes, *Org. Biomol. Chem.* 7 (2009) 4886–4894.
- [36] G. Miao, J. Ma, K. Yang, Z. Huang, Q. Gu, Y. Wang, Q. Guo, Q. You, J. Wang, Synthesis and bioevaluation of novel oxa-caged *Garcinia* xanthenes as anti-tumour agents, *Aust. J. Chem.* 68 (2015) 872–880.
- [37] H. Sun, F. Chen, X. Wang, Z. Liu, Q. Yang, X. Zhang, J. Zhu, L. Qiang, Q. Guo, Q. You, Studies on gambogic acid (IV): exploring structure-activity relationship with I κ B kinase-beta (IKK β), *Eur. J. Med. Chem.* 51 (2012) 110–123.
- [38] X. Wang, N. Lu, Q. Yang, D. Gong, C. Lin, S. Zhang, M. Xi, Y. Gao, L. Wei, Q. Guo, Q. You, Studies on chemical modification and biology of a natural product, gambogic acid (III): determination of the essential pharmacophore for biological activity, *Eur. J. Med. Chem.* 46 (2011) 1280–1290.
- [39] K.M. Elbel, G. Guizzunti, M.A. Theodoraki, J. Xu, A. Batova, M. Dakanali, E.A. Theodorakis, A-ring oxygenation modulates the chemistry and bioactivity of caged Garcinia xanthenes, *Org. Biomol. Chem.* 11 (2013) 3341–3348.
- [40] F. Bai, F. Morcos, Y.S. Sohn, M. Darash-Yahana, C.O. Rezende, C.H. Lipper, M.L. Paddock, L.H. Song, Y.T. Luo, S.H. Holt, S. Tamir, E.A. Theodorakis, P.A. Jennings, J.N. Onuchic, R. Mittler, S. Nechushtai, The Fe-S cluster-containing NEEET proteins mitoNEET and NAF-1 as chemotherapeutic targets in breast cancer, *Proc. Natl. Acad. Sci. U.S.A.* 112 (2015) 3698–3703.
- [41] M.A. Theodoraki, C.O. Rezende Jr., O. Chantarasriwong, A.D. Corben, E.A. Theodorakis, M.L. Alpaugh, Spontaneously-forming spheroids as an in vitro cancer cell model for anticancer drug screening, *Oncotarget* 6 (2015) 21255–21267.
- [42] S. Chia, S.M. Swain, D.R. Byrd, D.A. Mankoff, Locally advanced and inflammatory breast cancer, *J. Clin. Oncol.* 26 (2008) 786–790.
- [43] K.W. Hance, W.F. Anderson, S.S. Devesa, H.A. Young, P.H. Levine, Trends in inflammatory breast carcinoma incidence and survival: the surveillance, epidemiology, and end results program at the National Cancer Institute, *J. Natl. Cancer Inst.* 97 (2005) 966–975.
- [44] C.G. Kleer, K.L. van Golen, S.D. Merajver, Molecular biology of breast cancer metastasis. Inflammatory breast cancer: clinical syndrome and molecular determinants, *Breast Cancer Res.* 2 (2000) 423–429.
- [45] S. Sutherland, S. Ashley, G. Walsh, I.E. Smith, S.R. Johnston, Inflammatory breast cancer-The Royal Marsden Hospital experience: a review of 155 patients treated from 1990 to 2007, *Cancer* 116 (2010) 2815–2820.
- [46] D.J. van Uden, H.W. van Laarhoven, A.H. Westenberg, J.H. de Wilt, C.F. Blanken-Peters, Inflammatory breast cancer: an overview, *Crit. Rev. Oncol. Hematol.* 93 (2015) 116–126.
- [47] S. Dawood, N.T. Ueno, M. Cristofanilli, The medical treatment of inflammatory breast cancer, *Semin. Oncol.* 35 (2008) 64–71.
- [48] N. T. Ueno, M. Cristofanilli, Springer, Dordrecht ; New York, 2012, pp. 1 online resource (vi, 294 pages) illustrations (some color).
- [49] H. Yamauchi, W.A. Woodward, V. Valero, R.H. Alvarez, A. Lucci, T.A. Buchholz, T. Iwamoto, S. Krishnamurthy, W. Yang, J.M. Reuben, G.N. Hortobagyi, N.T. Ueno, Inflammatory breast cancer: what we know and what we need to learn, *Oncol.* 17 (2012) 891–899.
- [50] O.N. Kryvenko, J.I. Epstein, Histologic criteria and pitfalls in the diagnosis of lymphovascular invasion in radical prostatectomy specimens, *Am. J. Surg. Pathol.* 36 (2012) 1865–1873.
- [51] W.Y. Park, N. Shin, J.Y. Kim, T.Y. Jeon, G.H. Kim, H. Kim, D.Y. Park, Pathologic definition and number of lymphovascular emboli: impact on lymph node metastasis in endoscopically resected early gastric cancer, *Hum. Pathol.* 44 (2013) 2132–2138.
- [52] K. Tezuka, N. Onoda, T. Takashima, K. Takagaki, T. Ishikawa, T. Wakasa, K. Wakasa, K. Hirakawa, Prognostic significance of lymphovascular invasion diagnosed by lymphatic endothelium immunostaining in breast cancer patients, *Oncol. Rep.* 17 (2007) 997–1003.
- [53] Y. Yang, Y. Choi, S.H. Beom, J.W. Kim, Y.K. Joen, N.J. Kim, J.H. Kim, S.A. Im, K.H. Lee, A case report of breast cancer with extensive pulmonary lymphovascular tumor emboli, *Breast Canc. J.* 15 (2012) 128–132.
- [54] J. Morales, M.L. Alpaugh, Gain in cellular organization of inflammatory breast cancer: a 3D in vitro model that mimics the in vivo metastasis, *BMC Canc.* 9 (2009) 462.
- [55] E.J. Tisdale, I. Slobodov, E.A. Theodorakis, Biomimetic total synthesis of forbesione and desoxymorellin utilizing a tandem Claisen/Diels-Alder/Claisen rearrangement, *Org. Biomol. Chem.* 1 (2003) 4418–4422.
- [56] Z.-L. Liu, X.-J. Wang, N.-G. Li, H.-P. Sun, J.-X. Wang, Q.-D. You, Total synthesis of aldehyde-containing Garcinia natural products isomorellin and gaudichaudione A, *Tetrahedron* 67 (2011) 4774–4779.
- [57] E.J. Tisdale, I. Slobodov, E.A. Theodorakis, Unified synthesis of caged Garcinia natural products based on a site-selective Claisen/Diels-Alder/Claisen rearrangement, *Proc. Natl. Acad. Sci. U. S. A.* 101 (2004) 12030–12035.
- [58] M.G. Gichinga, S. Striegler, Regioselective alkylation of hydroxylsalicylaldehydes, *Tetrahedron* 65 (2009) 4917–4922.
- [59] S. P. Govek, M. Kahraman, S. Labadie, J. Li, J. Liang, J. Y. Nagasawa, D. F. Ortwine, N. D. Smith, X. Wang, J. Zbieg, F. Hoffmann-La Roche AG, Switz.; Genentech, Inc. . 2016, p. 221pp.
- [60] H. Tohma, H. Morioka, Y. Harayama, M. Hashizume, Y. Kita, Novel and efficient synthesis of p-quinones in water via oxidative demethylation of phenol ethers using hypervalent iodine(III) reagents, *Tetrahedron Lett.* 42 (2001) 6899–6902.
- [61] M.B. Andrus, E.J. Hicken, E.L. Meredith, B.L. Simmons, J.F. Cannon, Selective synthesis of the para-quinone region of geldanamycin, *Org. Lett.* 5 (2003) 3859–3862.
- [62] K.C. Nicolaou, P.K. Sasmal, H. Xu, Biomimetically inspired total synthesis and structure activity relationships of 1-O-methylateriflorone. 6 pi electrocyclicizations in organic synthesis, *J. Am. Chem. Soc.* 126 (2004) 5493–5501.
- [63] M.L. Alpaugh, S.H. Barsky, Reversible model of spheroid formation allows for high efficiency of gene delivery ex vivo and accurate gene assessment in vivo, *Hum. Gene Ther.* 13 (2002) 1245–1258.
- [64] C.A. Schneider, W.S. Rasband, K.W. Eliceiri, NIH Image to ImageJ: 25 years of image analysis, *Nat. Methods* 9 (2012) 671–675.
- [65] O. Thoison, D.D. Cuong, A. Gramain, A. Chiaroni, N.V. Hung, T. Sevenet, Further rearranged prenylxanthenes and benzophenones from *Garcinia bracteata*, *Tetrahedron* 61 (2005) 8529–8535.
- [66] O. Thoison, J. Fahy, V. Dumontet, A. Chiaroni, C. Riche, M.V. Tri, T. Sevenet, Cytotoxic prenylxanthenes from *Garcinia bracteata*, *J. Nat. Prod.* 63 (2000) 441–446.
- [67] H. Al-Ali, The evolution of drug discovery: from phenotypes to targets, and back, *Med. Chem. Comm.* 7 (2016) 788–798.
- [68] Y. Fang, R.M. Eglén, Three-dimensional cell cultures in drug discovery and development, *SLAS Discov.* 22 (2017) 456–472.
- [69] M.E. Katt, A.L. Placone, A.D. Wong, Z.S. Xu, P.C. Seanson, In vitro tumor models: advantages, disadvantages, variables, and selecting the right platform, *Front. Biotechnol. Bioeng.* 4 (2016) 12.
- [70] S.A. Langhans, Three-dimensional in vitro cell culture models in drug discovery and drug repositioning, *Front. Pharmacol.* 9 (2018) 6.
- [71] S. Sant, P.A. Johnston, The production of 3D tumor spheroids for cancer drug discovery, *Drug Discov. Today Technol.* 23 (2017) 27–36.
- [72] M. Zanoni, F. Piccinini, C. Arienti, A. Zamagni, S. Santi, R. Polico, A. Bevilacqua, A. Tesei, 3D tumor spheroid models for in vitro therapeutic screening: a systematic approach to enhance the biological relevance of data obtained, *Sci. Rep.* 6 (2016) 19103.
- [73] S. Yano, K. Takehara, H. Tazawa, H. Kishimoto, Y. Urata, S. Kagawa, T. Fujiwara, R.M. Hoffman, Cell-cycle-dependent drug-resistant quiescent cancer cells induce tumor angiogenesis after chemotherapy as visualized by real-time FUCCI imaging, *Cell Cycle* 16 (2017) 406–414.
- [74] J.A. Aguirre-Ghiso, M.S. Sosa, Emerging topics on disseminated cancer cell dormancy and the paradigm of metastasis, *Annu. Rev. Cell Biol.* 2 (2018) 377–393.
- [75] L.C. Klein-Júnior, R. Corrêa, Y. Vander Heyden, V. Cechinel Filho, All that glitters is not gold: panning cytotoxic natural products and derivatives with a fused tricyclic backbone by the estimation of their leadlikeness for cancer treatment, *Eur. J. Med. Chem.* 166 (2019) 1–10.